Substituent-Induced Intermolecular Interaction in Organic Crystals Revealed by Precise Band-Dispersion Measurements

Hiroyuki Yamane* and Nobuhiro Kosugi
Institute for Molecular Science, Myodaiji, Okazaki 444-8585, Japan
(Received 9 May 2013; published 21 August 2013)

We reveal quite small but different intermolecular valence band dispersions of sub-100-meV scale in crystalline films of Zn and Mn phthalocyanine (ZnPc and MnPc) and fluorinated ZnPc (F_{16}ZnPc). The intermolecular transfer integrals are found to be reasonably dependent on the intermolecular distance with the 75 ± 5 meV/Å relation. Furthermore, the angle-resolved photoemission spectra show anomalous dispersive behaviors such as phase flips and local-dimerization-derived periodicities, which originate from the site-specific intermolecular interaction induced by substituents.

DOI: 10.1103/PhysRevLett.111.086602 PACS numbers: 72.80.Le, 71.38.−k, 73.20.At, 79.60.−i

Organic semiconductors have attracted considerable interest for (opto)electronics based on the degree of freedom of molecules. Solid-state functionalities of such organic semiconductors are dominated not only by individual molecular properties but also by their intermolecular interactions. This concerted interplay governs a key process of the electric conduction in organic electronics, which consists of the charge injection at interfaces near the Fermi level (E_F) [1–3] and the charge transport in organic solids [4]. The coherence of the charge transport is dominated by the intermolecular coupling of individual molecular orbitals, depending on various conformations. In this Letter, we discuss the electronic band dispersion, i.e., energy versus wave vector [$E(\boldsymbol{k})$], of organic solids with high experimental accuracy, which can assess charge transport properties and related phenomena.

The *intermolecular* $E(\boldsymbol{k})$ relation, originating from the periodicity of the molecular stacking structure, is in general difficult to observe precisely. This is because a very small bandwidth due to the weak intermolecular interaction is easily obscured by structural and thermal energy broadenings. Therefore, the intermolecular $E(\boldsymbol{k})$ relation has been mainly reported for high hole-mobility (μ_h) materials with relatively large bandwidths (≥ 0.2 eV) [5–10]. Even in these cases, however, the intermolecular $E(\boldsymbol{k})$ relation is dominated by charge transport properties of the target molecules themselves. Precise and systematic study on the intermolecular $E(\boldsymbol{k})$ relation has not yet been established as a universal role in organic semiconductors. Thus, the fundamental knowledge on the intermolecular interaction is still insufficient.

In the present work, by using angle-resolved photoemission spectroscopy (ARPES) with synchrotron radiation, we shed light on quite small intermolecular $E(\boldsymbol{k})$ relations of sub-100-meV scale in crystalline films of metal phthalocyanine (MPc, M = metal). Even though MPc molecules are archetypal hole-transport materials in organic photovoltaics, their (opto)electronic properties have not yet been fully understood in relation to the intermolecular interaction because of the small $E(\boldsymbol{k})$ relation, which is easily buried by energetic disorders. Such a small $E(\boldsymbol{k})$ relation has not yet attracted much attention due to the lack of credible experimental data; however, present precise $E(\boldsymbol{k})$ measurements on MPc with different terminal groups and central metals are found to be sensitive and essential to characterize the intermolecular interaction in terms of the intermolecular distance, the conformational geometry, and the orbital character. Such a systematic approach provides deeper insights into the nature of the intermolecular interaction, which further represents the importance of the site specificity in the intermolecular interaction as a possible origin of unique molecular electronic properties.

A precise measurement of the small intermolecular $E(\boldsymbol{k})$ relation was carried out for MPc crystalline films on Au(111). Since the interaction between the physisorbed molecule and Au(111) is relatively weak [11,12], the self-assembling behavior by the intermolecular interaction plays a crucial role in the film crystallinity and its morphology from the initial stage of the film growth.

MPc crystalline films were prepared by vacuum deposition of purified MPc powders at 2 Å/min onto the clean Au(111) surface at 300 K. The Au(111) substrate was cleaned by repeated cycles of Ar^+ sputtering and annealing at 700 K, as confirmed by a core-level and a Shockley-state photoemission, and LEED. For molecular films, the photoemission peaks show the thickness-dependent energy shift, originating from the photohole relaxation by surrounding mediums [13,14]. Thus, the MPc deposition was continued until the MPc-derived peaks were stabilized in energy with respect to the deposition amount. The deposited MPc films were subsequently annealed at 350–360 K, which is the optimized temperature for the fabrication of MPc-based photovoltaic cells [15]. This annealing induces the enhancement of the Au $4f$ photoemission peak as the result of the molecular aggregation by further crystallization. The sample crystallinity was characterized by N K-edge x-ray absorption spectroscopy (XAS), LEED, and *ex situ* CuKα x-ray diffraction (XRD) (see the Supplemental

Material [16]). The ARPES and XAS experiments were performed at a high-brilliant vacuum ultraviolet and soft x-ray in-vacuum linear-polarized undulator beam line 6U of UVSOR-III at the Institute for Molecular Science. The ARPES spectra were obtained by using a micro-channel-plate detector of a hemispherical electron energy analyzer (A1, MB Scientific). The total energy resolution of 13 meV and the angular resolution of 0.2° were used in the present work. In order to avoid the radiation damage of the sample, by incident photons during the ARPES measurements, we chose a different fresh sample position after every measurement.

The ZnPc molecules on Au(111) form a flat-lying crystalline film with the intermolecular distance along the surface normal ($a_\perp$) of 3.326 Å in a Stranski-Krastanov growth mode (see the Supplemental Material [16]). In order to investigate the $E(\boldsymbol{k})$ relation in the π-π stacking direction, the normal-emission ARPES spectra as a function of the photon energy ($h\nu$) were measured for the ZnPc crystalline film at the specimen temperature (T) of 15 K [Fig. 1(a)]. Because of the growth mode of the ZnPc molecule on Au(111), the small remanent substrate E_F appears and is utilized for the energy calibration for the precise $E(\boldsymbol{k}_\perp)$ measurement. The ZnPc-derived peaks, labeled highest occupied molecular orbital (HOMO) and π, show a small but clear dispersive behavior with $h\nu$. The HOMO peak appears at the binding energy (E_b) of 1.32 eV at $h\nu = 46$ eV. With increasing $h\nu$, the HOMO peak shifts to the higher E_b side, and turns back at $h\nu = 58$ eV. Such an inflection point is also found around $h\nu = 90$ and 130 eV.

After converting to $\boldsymbol{k}_\perp$ from $h\nu$ in the second derivative of the ARPES spectra, the $E(\boldsymbol{k}_\perp)$ map for the ZnPc crystalline film at 15 K is obtained [Fig. 1(b)]. For the $\boldsymbol{k}_\perp$ conversion, we used an inner potential of -1.0 eV, based on the low-energy electron transmission experiment on α-CuPc [17]. The weak shoulder structure in the ARPES spectra around $E_b = 2.2$ eV is resolved in the $E(\boldsymbol{k}_\perp)$ map as labeled HOMO-1 and is derived from a Zn $3d_{x^2-y^2}$ orbital with the b_{1g} symmetry [18]. In the $E(\boldsymbol{k}_\perp)$ map, the HOMO, HOMO-1, and π peaks show the dispersion with the same $\boldsymbol{k}_\perp$ periodicity. The inflection points in the periodic dispersion correspond to the Γ and Y points in the Brillouin zone of the ZnPc crystalline film, as determined from $a_\perp = 3.326$ Å by XRD. This agreement proves that the observed periodic dispersion is ascribed to the delocalized band formation due to the weak intermolecular van der Waals (vdW) interaction. The one-dimensional tight-binding fitting, $E(\boldsymbol{k}_\perp) = E_b^0 - 2t_\perp \cos(a_\perp \boldsymbol{k}_\perp)$, as shown by white curves in the $E(\boldsymbol{k}_\perp)$ map, to the HOMO-band dispersion at 15 K gives the dispersion center (E_b^0) of 1.388 eV, the transfer integral ($t_\perp$) of 23 meV, and the resultant hole effective mass (m_h^*) of $15.0m_0$, where m_0 is the free-electron mass. The observed m_h^* gives the ideal μ_h of 26.6 $\mathrm{cm^2\,V^{-1}\,s^{-1}}$ for the HOMO of α-ZnPc crystals at 15 K from $\mu_h > 20(m_0/m_h^*)(300/T)$ [5].

In α-ZnPc crystals, two nonequivalent molecules in the unit cell should induce the HOMO-band splitting, as

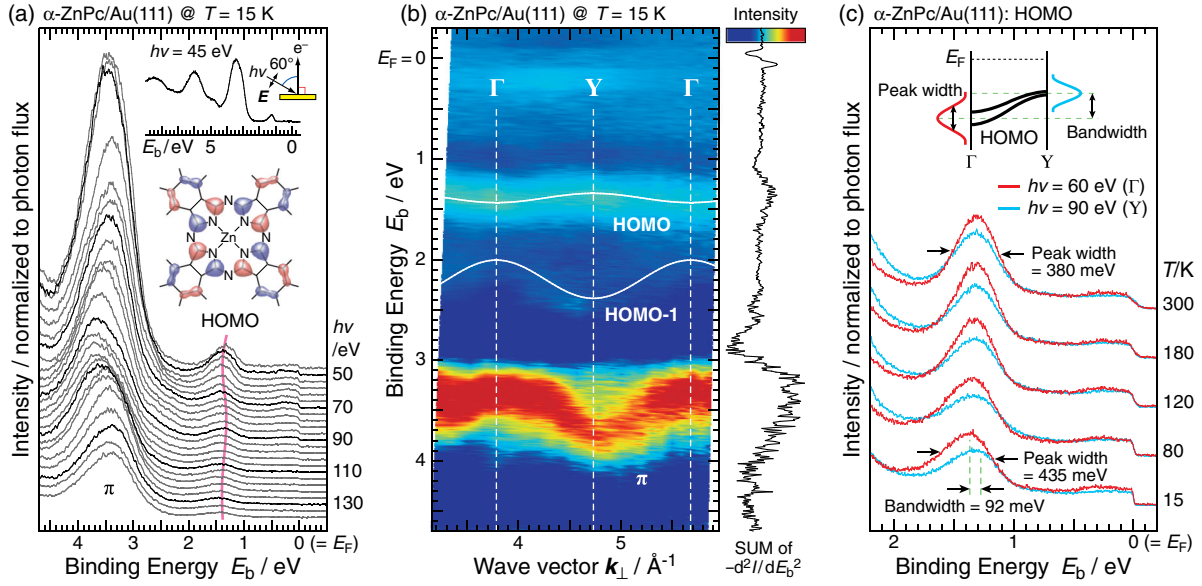

FIG. 1 (color online). Intermolecular $E(\boldsymbol{k})$ relation in the ZnPc crystalline film on Au(111). (a) $h\nu$-dependent normal-emission ARPES spectra at 15 K ($h\nu$ step = 4 eV). The experimental geometry, wide valence-band spectrum at $h\nu = 45$ eV, and the linear combination of atomic orbitals (LCAO) pattern of the HOMO of ZnPc are also shown. (b) $E(\boldsymbol{k}_\perp)$ map obtained from the second derivative of the ARPES spectra ($-d^2I/dE_b^2$), with the tight-binding fitting (white curve). Sum of the $-d^2I/dE_b^2$ spectra is shown in the right side of the $E(\boldsymbol{k}_\perp)$ map. (c) T dependence of the HOMO band at the Γ and Y points, measured at $h\nu = 60$ and 90 eV, respectively. The HOMO-band dispersion is illustrated in the inset.

observed for pentacene and rubrene with the split energy of ~0.4 eV by relatively strong intermolecular interaction [7–9]. In the present case of ZnPc, however, the HOMO-band splitting is not resolved by the weak intermolecular interaction. It might be reflected in the T-dependent width and energy of the HOMO peak according to the small polaron theory based on the electron-phonon (e-ph) coupling [19,20]. Figure 1(c) shows the T-dependent HOMO peak at the Γ and Y points, measured at $h\nu = 60$ and 90 eV, respectively. The Γ-point HOMO shifts to the lower E_b side with increasing T, while the Y-point HOMO does not shift, indicating the narrowing of the bandwidth at higher T. Furthermore, only the Γ-point HOMO shows a peak width narrowing with increasing T (435 meV at 15 K and 380 meV at 300 K), which is the opposite trend of the thermal broadening in the remanent substrate E_F. This evidence indicates that the Γ-point HOMO is weakly split at 15 K. Here, the bandwidth ($4t_\perp$) of 92 meV at 15 K is of the same order as the reorganization energy for local phonons in CuPc [21]. It is considered that the T-dependent transition between the incoherent hopping transport by the local e-ph coupling and the coherent band-like transport by the nonlocal e-ph coupling exists within the energy scale of 100 meV in α-ZnPc crystals.

Since functionalities of MPc can be modified by the chemical substitution of terminal groups and central metals in the molecule, the present precise $E(\boldsymbol{k})$ observation for ZnPc is considered to be a starting system in carrying out a systematic study on the dependence of the intermolecular interaction. In this context, we prepared crystalline films of fluorinated ZnPc (F_{16}ZnPc) and MnPc on Au(111), obtained by the same sample preparation procedure for ZnPc. It is confirmed by XAS and XRD that the molecules form the β-bilayer (β_{BL})-crystalline phase [22,23] with $a_\perp = 3.236$ Å for F_{16}ZnPc and the α-crystalline phase with $a_\perp = 3.273$ Å for MnPc (see the Supplemental Material [16]).

As shown in the inset of Fig. 2(a), the HOMO of F_{16}ZnPc is derived from the C $2p$ and F $2p$ orbitals with a_{1u} symmetry. Different intermolecular interaction between F_{16}ZnPc and ZnPc is expected due to the F $2p$ orbital and the different $a_\perp$. The $h\nu$ dependence of the normal-emission ARPES spectra for the F_{16}ZnPc crystalline film on Au(111) at 15 K is shown in Fig. 2(a). The HOMO peak shows a clear dispersive behavior with $h\nu$. Figure 2(b) shows the $E(\boldsymbol{k}_\perp)$ map in the HOMO-band region of F_{16}ZnPc, in comparison with that of ZnPc. We found that the HOMO bandwidth of F_{16}ZnPc (120 meV) is larger than that of ZnPc (92 meV), which is reasonably explained by a shorter intermolecular distance $a_\perp = 3.236$ Å for F_{16}ZnPc than $a_\perp = 3.326$ Å for ZnPc.

A more important result in Fig. 2(b) is the difference in the HOMO dispersion phase between ZnPc and F_{16}ZnPc crystalline films. From the Γ to Y point, the HOMO band of ZnPc disperses to the lower E_b side, in agreement with the

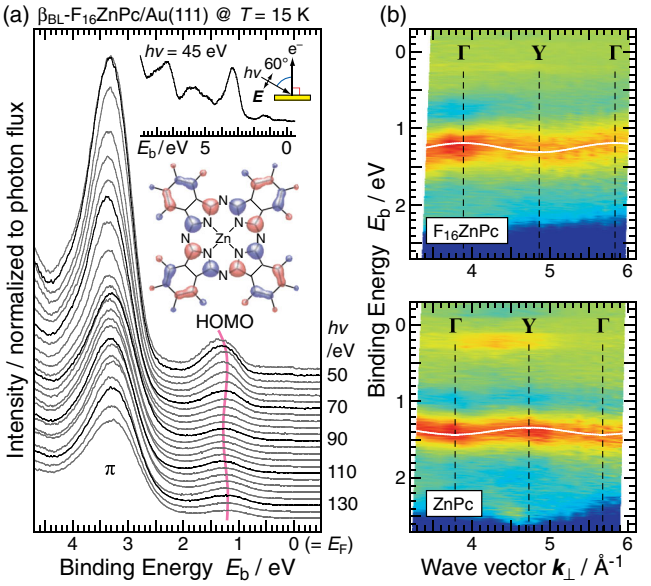

FIG. 2 (color online). (a) $h\nu$-dependent normal-emission ARPES spectra ($h\nu$ step = 4 eV) of the F_{16}ZnPc crystalline film on Au(111) at 15 K. The experimental geometry, wide valence-band spectrum at $h\nu = 45$ eV, and the LCAO pattern of the HOMO of F_{16}ZnPc are also shown. (b) $E(\boldsymbol{k}_\perp)$ map of the HOMO band for crystalline films of F_{16}ZnPc and ZnPc, obtained from the second derivative of the ARPES spectra, with the tight-binding fitting (white curve).

calculated band structure of α-CuPc [24]. On the other hand, the HOMO dispersion direction of F_{16}ZnPc is flipped from that of ZnPc. The observed $E(\boldsymbol{k})$-phase flip may originate from the modification of the intermolecular HOMO overlap between ZnPc and F_{16}ZnPc due to the different conformational structure and an intermolecular interaction between Pc π and F $2p$.

The next modification is on the central metal, MnPc. The HOMO of MnPc is derived from the half filled Mn $3d$ orbital with e_g symmetry, and the HOMO-1 of MnPc corresponds to the HOMO of ZnPc [25–27]. The half filled HOMO of MnPc induces the crystallinity-dependent magnetic properties [28]. Figure 3(a) shows the $h\nu$ dependence of the normal-emission ARPES spectra for the MnPc crystalline film on Au(111) at 15 K. The relative intensity between the HOMO (Mn $3d$) and HOMO-1 (C $2p$) peaks changes with $h\nu$ due to different ionization cross sections. The Mn $3d$ and C $2p$ peaks show a clear dispersive behavior with $h\nu$. Moreover, the Mn $3d$ peak consists of two components, indicating the relatively strong interaction at the Mn site. Figure 3(b) shows the $E(\boldsymbol{k}_\perp)$ map for the MnPc crystalline film on Au(111) at 15 K, wherein the Γ and Y points are estimated from $a_\perp = 3.273$ Å (see the Supplemental Material [16]). The agreement between the periodicity of the C $2p$ dispersion and the Brillouin zone indicates that the observed C $2p$ dispersion is ascribed to the intermolecular vdW interaction. From the tight-binding fitting, we found that the bandwidth for the C

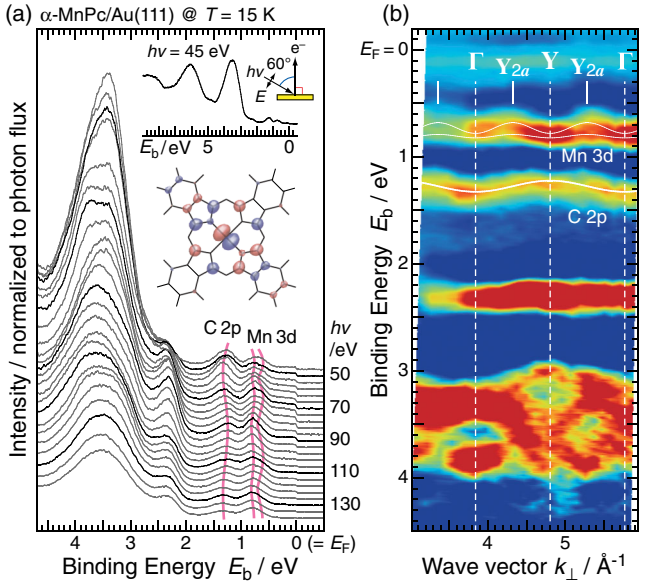

FIG. 3 (color online). (a) $h\nu$-dependent normal-emission ARPES spectra ($h\nu$ step = 4 eV) of the MnPc crystalline film on Au(111) at 15 K. The experimental geometry, wide valence-band spectrum at $h\nu = 45$ eV, and the LCAO pattern of the HOMO of MnPc are also shown. (b) $E(\boldsymbol{k}_\perp)$ map obtained from the second derivative of the ARPES spectra, with the tight-binding fitting (white curve).

$2p$ band of MnPc (104 meV) is between ZnPc (92 meV) and F_{16}ZnPc (120 meV), which is consistent with $a_\perp = 3.273$ Å for MnPc between $a_\perp = 3.326$ Å for ZnPc and $a_\perp = 3.236$ Å for F_{16}ZnPc.

For the Mn $3d$ peak, the peak splitting and its dispersion are resolved in the $E(\boldsymbol{k}_\perp)$ map. The $\boldsymbol{k}_\perp$ periodicity of the Mn $3d$ dispersion is $1/2$ times that of the C $2p$ dispersion as labeled Y_{2a} and is simply thought to originate from the local dimerization and the resultant double-$a_\perp$-periodicity modulation at the Mn site. Such evidence is not observable for the full-filled Co $3d$ peak of the CoPc crystalline film (see the Supplemental Material [16]), suggesting the importance of the half filled orbital character. This is an indication of the strong electron correlation at the Mn site, which induces the smaller m_h^* of $3.6m_0$ for the topmost Mn $3d$ band as well as the antiferromagnetism found for the MnPc crystalline film [28].

TABLE I. The energy of the dispersion center E_b^0 (eV), the transfer integral $t_\perp$ (meV), the hole effective mass m_h^*, and the hole mobility μ_h ($\mathrm{cm^2\,V^{-1}\,s^{-1}}$) for the C $2p$ derived band of ZnPc, MnPc, and F_{16}ZnPc crystalline films at 15 K, together with their intermolecular distance $a_\perp$ (Å).

	$a_\perp$	E_b^0	$t_\perp$	m_h^*	μ_h
ZnPc	3.326	1.388	23	$15.0m_0$	26.6
MnPc	3.273	1.274	26	$13.7m_0$	29.2
F_{16}ZnPc	3.236	1.251	30	$12.2m_0$	32.9

As summarized in Table I, we have succeeded in observation of the intermolecular $E(\boldsymbol{k})$ relations of sub-100-meV scale in crystalline films of various MPc molecules. Here, F_{16}CuPc (similar to F_{16}ZnPc) solids show the optical absorption at 688 nm for the β_{BL} phase and at 780 nm for the β phase [23]. On the other hand, CuPc solids show the optical absorption at 687 nm for the α phase and at 714 nm for the β phase [29]. Since the optical absorption on MPc solids is sensitive to intermolecular transition dipole moments, it is considered that the crystalline structure of β_{BL}-F_{16}ZnPc resembles that of α-ZnPc rather than β-ZnPc. Furthermore, the LEED pattern of the F_{16}ZnPc film corresponds to that of other nonfluorinated MPc films (see the Supplemental Material [16]), supporting the similarity of the crystalline structure between β_{BL}-F_{16}ZnPc and α-ZnPc. Although a little contribution of the F $2p$ orbital on the C $2p$ bandwidth of F_{16}ZnPc exists, the $t_\perp$-versus-$a_\perp$ relation for the C $2p$ band of MPc can be linearly fitted in the present $a_\perp$ range with $t_\perp/a_\perp = 75 \pm 5$ meV/Å, as shown in Fig. 4. This parameter can be a reference for the refinement of theoretical calculations on the intermolecular vdW interaction, which sometimes over- or underestimate the bandwidth.

In addition to the systematic characterization of the $E(\boldsymbol{k})$ width, based on the sensitivity of the small $E(\boldsymbol{k})$ relation to surrounding environments, we observed changes in the $E(\boldsymbol{k})$ phase and the $\boldsymbol{k}$ periodicity by the substitution of terminal groups and central metals in MPc, e.g., (i) the $E(\boldsymbol{k})$-phase flip of the HOMO band between ZnPc and F_{16}ZnPc, and (ii) the double-periodicity modulation for the half filled Mn $3d$ band of MnPc. These anomalous behaviors in the intermolecular $E(\boldsymbol{k})$ relation can be explained by the presence of the site-specific intermolecular interaction due to substituents in MPc, which induces miscellaneous electronic and magnetic properties. The present results clearly indicate that, even in single-component molecular systems, strong local electron correlations can be introduced by the molecular design and its local intermolecular interaction.

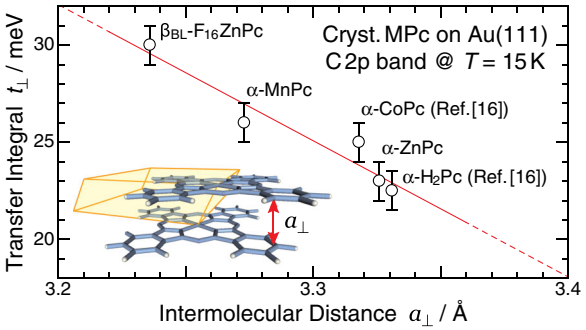

FIG. 4 (color online). The $t_\perp$-versus-$a_\perp$ relation for the C $2p$ band in MPc crystals at 15 K. Experimental data for CoPc and H_2Pc are given in the Supplemental Material [16].

As demonstrated above, precise and systematic intermolecular $E(\boldsymbol{k})$ measurements on various organometallic complexes enable us to reveal different intermolecular interactions quantitatively and to obtain a quantitative guiding principle for the design of functional molecular systems and their theoretical considerations from the viewpoint of the intermolecular interaction in addition to the individual molecular property, as a critical tool for organic electronics.

We thank the staff of the UVSOR facility for their kind support, in particular, T. Horigome in the development of the ARPES system. We also thank T. Hosokai (Iwate University) for fruitful discussion on the crystalline structure of F_{16}ZnPc. This work was partly supported by Grants-in-Aid for Scientific Research (A) (No. 23245007) and for Young Scientists (A) (No. 24685032) from JSPS.

*Corresponding author.
yamane@ims.ac.jp

[1] H. Ishii, K. Sugiyama, E. Ito, and K. Seki, Adv. Mater. **11**, 605 (1999).
[2] A. Kahn, N. Koch, and W. Gao, J. Polym. Sci., Part B: Polym. Phys. **41**, 2529 (2003).
[3] S. Braun, W. R. Salaneck, and M. Fahlman, Adv. Mater. **21**, 1450 (2009).
[4] V. Coropceanu, J. Cornil, D. A. da Silva Filho, Y. Olivier, R. Silbey, and J. L. Brédas, Chem. Rev. **107**, 926 (2007).
[5] N. Ueno and S. Kera, Prog. Surf. Sci. **83**, 490 (2008), and references therein.
[6] G. Koller, S. Berkebile, M. Oehzelt, P. Puschnig, C. Ambrosch-Draxl, F. P. Netzer, and M. G. Ramsey, Science **317**, 351 (2007).
[7] H. Kakuta, T. Hirahara, I. Matsuda, T. Nagao, S. Hasegawa, N. Ueno, and K. Sakamoto, Phys. Rev. Lett. **98**, 247601 (2007).
[8] S. I. Machida, Y. Nakayama, S. Duhm, Q. Xin, A. Funakoshi, N. Ogawa, S. Kera, N. Ueno, and H. Ishii, Phys. Rev. Lett. **104**, 156401 (2010).
[9] S. Ciuchi, R. C. Hatch, H. Höchst, C. Faber, X. Blase, and S. Fratini, Phys. Rev. Lett. **108**, 256401 (2012).
[10] Q. Xin, S. Duhm, F. Bussolotti, K. Akaike, Y. Kubozono, H. Aoki, T. Kosugi, S. Kera, and N. Ueno, Phys. Rev. Lett. **108**, 226401 (2012).
[11] G. Witte and C. Wöll, J. Mater. Res. **19**, 1889 (2011).
[12] I. Kröger, B. Stadtmüller, C. Wagner, C. Weiss, R. Temirov, F. S. Tautz, and C. Kumpf, J. Chem. Phys. **135**, 234703 (2011).
[13] H. Peisert, M. Knupfer, T. Schwieger, J. M. Auerhammer, M. S. Golden, and J. Fink, J. Appl. Phys. **91**, 4872 (2002).
[14] H. Yamane, Y. Yabuuchi, H. Fukagawa, S. Kera, K. K. Okudaira, and N. Ueno, J. Appl. Phys. **99**, 093705 (2006).
[15] K. Suemori, T. Miyata, M. Hiramoto, and M. Yokoyama, Jpn. J. Appl. Phys. **43**, L1014 (2004).
[16] See Supplemental Material at http://link.aps.org/supplemental/10.1103/PhysRevLett.111.086602 for extra supporting data.
[17] N. Ueno, K. Sugita, and T. Shinmura, Phys. Rev. B **44**, 6472 (1991).
[18] M.-S. Liao and S. Scheiner, J. Chem. Phys. **114**, 9780 (2001).
[19] K. Hannewald, V. M. Stojanović, J. M. T. Schellekens, P. A. Bobbert, G. Kresse, and J. Hafner, Phys. Rev. B **69**, 075211 (2004).
[20] C. A. Perroni, V. Marigliano Ramaglia, and V. Cataudella, Phys. Rev. B **84**, 014303 (2011).
[21] S. Kera, H. Yamane, and N. Ueno, Prog. Surf. Sci. **84**, 135 (2009).
[22] D. G. de Oteyza, E. Barrena, J. O. Ossó, S. Sellner, and H. Dosch, J. Am. Chem. Soc. **128**, 15052 (2006).
[23] T. Hosokai, A. Gerlach, A. Hinderhofer, C. Frank, G. Ligorio, U. Heinemeyer, A. Vorobiev, and F. Schreiber, Appl. Phys. Lett. **97**, 063301 (2010).
[24] G. Giovannetti, G. Brocks, and J. van den Brink, Phys. Rev. B **77**, 035133 (2008).
[25] M.-S. Liao, J. D. Watts, and M.-J. Huang, Inorg. Chem. **44**, 1941 (2005).
[26] M. Grobosch, B. Mahns, C. Loose, R. Friedrich, C. Schmidt, J. Kortus, and M. Knupfer, Chem. Phys. Lett. **505**, 122 (2011).
[27] F. Petraki, H. Peisert, P. Hoffmann, J. Uihlein, M. Knupfer, and T. Chassé, J. Phys. Chem. C **116**, 5121 (2012).
[28] H. Yamada, T. Shimada, and A. Koma, J. Chem. Phys. **108**, 10 256 (1998).
[29] H. Yoshida, Y. Tokura, and T. Koda, Chem. Phys. **109**, 375 (1986).